Article

RNAi-mediated down-regulation of Dicer-like 2 and 4 changes the response of "Moneymaker" tomato to potato spindle tuber viroid infection from tolerance to lethal systemic necrosis, accompanied by up-regulation of miR398a-3p and reactive oxygen species

Takahiro Suzuki[1,2], Sho Ikeda[1], Atsushi Kasai[1], Akito Taneda[3], Kohei Sugawara[1], Misato Fujibayashi[1], Maki Okuta[1], Hayato Maeda[1], Teruo Sano[1]

[1]Faculty of Agriculture and Life Science, Hirosaki University, Bunkyo-cho 3, Hirosaki 036-8561, Japan
[2]Union Graduate school of Agricultural Sciences, Iwate University, 3-18-8 Ueda, Morioka, Iwate 020-8550, Japan
[3]Graduate School of Science and Technology, Hirosaki University, Bunkyo-cho 3, Hirosaki 036-8561, Japan

Abstract: To examine the role of RNA silencing in defense against viroid, a Dicer-like 2 and 4 (DCL2&4) – double knockdown transgenic tomato line 72E was created. The expression of endogenous DCL2 and DCL4 in line 72E decreased to about a half of the empty cassette line EC. When challenged with potato spindle tuber viroid (PSTVd), 72E allowed significantly higher level of PSTVd accumulation early in infection and showed lethal systemic necrosis. The size distribution of PSTVd-derived small RNA was significantly changed: the numbers of 21 and 22 nucleotides (nt) species in line 72E was approximately 66.7% and 5% of those in line EC, respectively. Conversely, the numbers of 24-nt species increased by 1100%. Furthermore, expression of miR398a-3p and miR398 increased 770–868% in the PSTVd-infected 72E, compared to the PSTVd-infected EC. In parallel, superoxide dismutase (SOD1) in PSTVd-infected 72E showed higher expression levels. In concert with miR398a-3p, SOD1 controls detoxification of reactive oxygen species (ROS) generated in cells. Since high levels of ROS production and its scavenging activity were observed in PSTVd-infected 72E, the lack of full-activity of DCLs was thought to have made the plant incapable to control excessive ROS production and thus resulted in to develop lethal systemic necrosis.

Keywords: viroid; pathogenicity; RNA silencing; Dicer-like proteins; small interfering RNA; microRNA398; microRNA398a-3p; superoxide dismutase 1; reactive oxygen species; systemic necrosis

Introduction

Viroids are the smallest known pathogens of higher plants [1]. They consist solely of a highly-structured covalently closed circular RNA that range between 246 and 434 nucleotides (nt) in length. The species reported so far (more than 30) are classified into two genera, *Pospiviroidae* and *Avsunviroidae*, depending on the characteristics of their nucleotide sequence, mode of replication, subcellar localization, host specificity, and specific disease symptoms [2]. Viroids replicate autonomously in the nucleus or chloroplasts of invaded host cells, depending completely on the host's transcription machinery. Some cause mild to severe disease in sensitive hosts, while other infections are asymptomatic. In light of the non-coding nature of the viroid genome, all the factors necessary to replicate in invaded host cells (i.e., to recuruit transcription machinery such as *Pol II* and transcription factors, to move from cell to cell, and to spread systemically, and even those necessary

 doi:10.20944/preprints201811.0606.v1

to cause disease symptoms) must be embeded in the highly base-paired stem-loop structure [3]. However, many of these properties are yet to be studied and described.

Potato spindle tuber viroid (PSTVd) species of the genus *Pospiviroid* was first identified in North America as the causal agent of spindle tuber disease in potato (*Solanum tuberosum*) [1]. Early studies show that PSTVd has a relatively wide experimental host range [4], and, in the early 21st century, natural infections of PSTVd in hosts other than potato were first reported in tomato and ornamentals of the families *Solanaceae* and *Asteraceae* [5–7]. Other pospiviroids in addition to PSTVd have begun to expand into new geographical areas through global distribution of contaminated seeds and vegetatively-propagated planting materials, thereby causing serious concerns in the seed industry, as well as plant quarantine, worldwide [8].

Tomato (*Solanum lycopersicum*) is the most sensitive host to PSTVd, but the severity of symptoms varies depending on the host cultivar, as well as the PSTVd variant. For example, in response to a severe isolate of PSTVd, a symptomatic cultivar "Rutgers" shows severe leaf curling and stunting, but a tolerant cultivar "Moneymaker" shows little or no stunting, although both accumulate a systemic abundance of PSTVd [9, 10]. Such variation in symptoms is believed to be determined by the difference in the genetic makeup of host cultivars in response to the infection of PSTVd variants with distinct molecular characteristics [11].

In response to pathogen attack, plants induce layers of defense responses called pathogen-associated molecular patterns (PAMPs)-triggered immunity (MTI) or effector-triggered immunity that involve the activation of various plant defense responses, including programmed cell death [12]. Among such defense responses, RNA-silencing functions to protect many eukaryotic genomes from invading viruses, foreign transgenes, and transposable elements [13–15]. For members of the family *Pospiviroidae* that replicate inside the nucleus in the host cells, double-stranded or highly-structured regions of RNA molecules synthesized during replication are recognized as PAMPS, thereby triggering attack by Dicer-like proteins (DCLs) located at the front line of defense and cleaved into viroid-derived small RNAs (vd-sRNA) consisting of 21- to 24-nt [9, 16–21]. Viroids in the family *Avsunviroidae* replicate in chloroplasts and are also targeted by DCLs and cleaved into small pieces (around 21- to 22-nt) [22–24]. Vd-sRNAs are then loaded onto Argonaute (AGO) proteins to form RNA-induced silencing complexes (RISCs), which target native viroid molecules by the guidance of vd-sRNAs and digest them into vd-sRNAs again by slicer activity of AGO proteins [25]. In the meantime, the digested viroid RNA called "aberrant RNA" is believed to be converted into double-stranded RNA by the action of RNA-dependent RNA polymerase 6 (RDR6) and, again, processed into small pieces by DCLs for the amplification of the silencing signal [26, 27]. Finally, the action of RNA-silencing mechanism leads to the accumulation of a large quantity of vd-sRNA in viroid-infected host plants, which is thought to play an important role in various aspects of viroid-host interaction, including defense [28–32], molecular evolution [33], and even symptom expression [33–40].

DCLs play a central role in the RNAi pathway and are key components in the biogenesis of small RNAs (sRNAs), called short interfering RNA (siRNA) and micro RNA (miRNA) [41]. Four DCLs have been described in plants: *viz*., DCL1, DCL2, DCL3, and DCL4 [42]. In *Arabidopsis thaliana*, DCL1 is involved in miRNA biogenesis and produces mature miRNAs 21-nt in length [43–45]. DCL2 generates stress-related 22-nt natural-antisense-transcript (nat)-siRNAs and 22-nt siRNAs of exogenous origin [46, 47] and are reported to process ~22-nt siRNAs from ta-siRNA precursors in the absence of DCL4 [48]. DCL2 (in combination with DCL4) is also involved in the production of secondary siRNAs that trigger a phenomenon known as "transitivity" [49] and play a role in the antiviral defense [46, 50, 51]. DCL3 produces 24-nt-long, DNA repeat–associated siRNAs that guide heterochromatin formation [46]. DCL4 generates 21-nt-long siRNAs that mediate post-transcriptional silencing of some endogenous genes (e.g., trans-acting (ta)–siRNAs) [48, 52] and of transgenes mediating RNA interference [53]. DCL4 is also responsible for processing specific miRNAs in *Arabidopsis thaliana* [54, 55] and has a role in transcriptional termination [56, 57] and antiviral defense mechanisms [50, 58, 59]. Among the various roles of DCL proteins, the action to counteract viruses and viroids is particularly interesting, because they are known to work cooperatively, but

hierarchically, to combat pathogens in invaded cells as the front line of defense. In particular, DCL2 and DCL4 play an important role in the defense against viruses [58, 60]. In addition, DCL1 has the potential to produce 21-nt viral siRNA in the absence of DCL2, DCL3, and DCL4 [50, 58].

Published data on the detection of vd-sRNAs in viroid-infected plants suggest that the highly base-paired stem-loop structure of viroids can serve as a substrate for multiple DCLs [9, 16–19, 22]. Direct evidence for such cleavage was first obtained from experiments that demonstrated that PSTVd RNA was cleaved into small pieces of ~21-nt when incubated with *Arabidposis spp.* cell extracts containing DCL activities [18]. A more detailed analysis using a series of *Nicotiana benthamiana DCL*-knockdown lines revealed that PSTVd levels dropped when either i) *DCL4* expression alone was suppressed or ii) *DCL1*, *DCL2*, or *DCL3* was knocked down together with *DCL4*. These observations led to a new hypothesis, that the combined activity of DCL2 and DCL3 is crucial in the defense against PSTVd [20, 21]. In this scenario, DCL4 is proposed to play the key role in processing PSTVd, and its activity may obscure or suppress the effects of DCL2/DCL3 on viroid infectivity, suggesting that hierarchical interactions among DCLs are also important in defense against viroids.

To analyse PSTVd pathogenicity in tomato from the standpoint of RNA silencing we have introduced an inverted-repeat (IR) chimera gene construct, consisting of parts of the tomato unigenes *DCL2* and *DCL4* into the tomato variety Moneymaker. We then challenged three lines of T3-generation plants by inoculation with PSTVd to examine the roles of DCL2 and DCL4 in the defense against viroid infection. In one of these lines (named line 72E), in which endogenous *DCL2* and *DCL4* mRNAs were down-regulated by transgene-derived RNA silencing, the response to PSTVd infection was changed from "tolerant" to "highly susceptible," and the infected plants displayed lethal systemic necrosis. Both deep sequencing analysis and RNA-gel blot hybridization revealed that the size distribution of vd-sRNAs had changed dramatically in PSTVd-infected 72E plants (PSTVd-72E). Furthermore, the expression level of two microRNA species (miR398 and 398a-3p) and cytosolic superoxide dismutase 1 copper chaperone (*SOD1*) mRNA was unusually higher in PSTVd-72E. Since *SOD1*, in concert with miR398a-3p, miR398 and superoxide dismutase *CCS1* (a target of miR398a-3p) [61], has a function to control detoxification of harmful reactive oxygen species (ROS) in the cell, RNAi-mediated down-regulation of *DCL2* and *DCL4* seemed to have resulted in failed initial defense against viroid infection, triggered excessive production of ROS, and resulted in the development of severe systemic necrosis.

MATERIALS AND METHODS

Generation of DCL2/4i transgenic tomato 'Moneymaker' lines

In order to knockdown *DCL2* and *DCL4* expression via RNAi, an IR sequence was constructed as follows, based on the sequence of tomato homologs of *A. thaliana DCL2* (Solyc06g048960, Solyc11g008530, Solyc11g008540) and *DCL4* (Solyc07g005030) registered in the tomato genome database (ttps://solgenomics.net/organism/ Solanum_lycopersicum/genome). The artificial chimera gene (SlartDCL2&4) was constructed by placing parts of *DCL2* (620 bp) and *DCL4* (300 bp) in head-to-head orientation across an intron sequence to create an IR sequence (Figure S1). SlartDCL2&4 IR was inserted into the *Sac*II/*Sal*I site of pBluescript II SK (+) plasmid (Agilent Technologies), re-cloned into the *Bgl*II/*Kpn*I site of binary vector pIG121-Hm [62] downstream of the CaMV-35S promoter (35S:SlartDCL2&4 IR), and introduced into *Agrobacterium tumefaciens* strain EHA105 to transform tomato cv Moneymaker by the leaf disc method [28]. Transformants (T0 generation) were selected on media containing kanamycin, transplanted to pots for further cultivation, and self-fertilized to produce the T1 generation. By repeating the kanamycin selection and self-fertilization, three lines (hpDCL2/4i-51-6, -72E, and -82a) of the T3-generation were selected. In addition, tomato plants transformed with pIG121-Hm containing an empty cassette were created and used as a negative control (line EC).

 doi:10.20944/preprints201811.0606.v1

Preparation of PSTVd inoculum and infection assay

Plasmid DNA (~2 µg) containing an infectious cDNA clone of PSTVd-Intermediate (pTZ18R-Rz6-PSTV; accession no. M16826) was linearized by *Not*I restriction enzyme digestion (Takara Bio, Otsu, Shiga, Japan) and used for *in vitro* transcription in a 20 µl reaction mixture containing T7 RNA polymerase (Invitrogen, Carlsbad, CA, USA) at 37°C for 2 hrs according to manufacturer's instruction. Inoculum was adjusted to a concentration of 100 ng of the transcript/µl in 50 mM sodium phosphate buffer (pH 7.5), 1 mg/ml bentonite. For mechanical inoculation, an aliquot (10 µl) was placed on the third true leaf of Moneymaker seedlings dusted with carborundum (600-mesh) and gently rubbed against the leaf 10 times using a sterile glass-bar. Ten seedlings each from four different hpDCL2/4i Moneymaker lines (i.e., empty cassette, 51-6, 72E and 82a) were used for each infection assay. After inoculation plants were incubated in a growth chamber controlled at 22ºC (night) – 30ºC (day), 16-h day-length supplemented with high intensity fluorescent light (40 watts × 4).

Preparation of total nucleic acids, genomic DNA, and total RNA from tomato plants

Accumulation of viroid in the inoculated plants were examined using total nucleic acids extracted by CTAB method [63]. Two leaf disks (1 cm in diameter, ~0.05 g) were collected from the upper most expanded leaves of each plant at two, three, and four weeks post inoculation (wpi), and homogenized in 0.5 ml of 2× CTAB buffer using a multi-specimen cell disruption device (Shake Master, BMS Co Ltd, Tokyo, Japan) with two zirconia-balls (φ=5 mm). Total nucleic acid pellets were dissolved in 50–100 µl distilled water.

The presence and the copy number of transgene was examined by detecting the CaMV-35S promoter sequence in genomic DNA preparations extracted from samples of leaf tissue. Total nucleic acids were extracted from homogenate prepared in 2× CTAB buffer (~1 g/5 ml) with equal volume (v/v) of phenol-chloroform (1:1), precipitated by ethanol, and resuspended in 100–400 µl distilled water. They were further incubated with RNaseA (DNase-free, Wako NIPPON GENE, Japan) at 37°C for 45 minutes (min) to digest RNAs, and ethanol-precipitated after extraction with phenol-chloroform. RNA-free genomic DNA pellets were dissolved in 100 µl distilled water.

Total RNA preparations required for analysis of transgene transcripts, siRNA derived from transgene transcripts, small RNAs for deep sequencing, and specific host gene expression, were extracted using Trizol (Thermo Fisher Scientific) or TriReagent (Molecular Research Center, Inc., Cincinnati OH, USA) according to the manufacturer's instruction.

Detection of CaMV-35S promoter sequence by PCR

Portions of the CaMV-35S promoter and actin gene sequences were amplified by PCR using 0.1 µg of total nucleic acids as template and analyzed by 7.5% polyacrylamide gel electrophoresis. PCR was performed using One Taq DNA polymerase (New England BioLabs Japan) according to the manufacturer's instruction and the appropriate primer set (see Table S1). The resulting PCR products were fractionated in 7.5% polyacrylamide gels containing 1×TAE buffer.

Southern-blot hybridization to analyse transgene copy number in transformed plants

Aliquots of genomic DNA (~15 µg) were digested with EcoRI or BamHI (Thermo Fisher Scientific K.K., Japan), electrophoresed at 50V (4V/cm) for 8 hours in 1.0% agarose gel (1×TAE buffer), transferred to a nylon membrane (Biodyne; Pall Corporation, Port Washington, NY, USA) after NaOH-denaturation followed by HCl-neutralization, and hybridized with a DIG-labeled cRNA probe for CaMV-35S promorter sequence. Hybridization signals were visualized using Chemidoc-XRS imaging system and quantified using the Quantity One (version 4.6.2) software package.

Northern-blot hybridization to analyze transgene transcripts, siRNA derived from transgene transcripts, vd-sRNAs, host gene expression, and miRNA

Total RNA preparations (1~10 µg) extracted using Trizol or TriReagent were denatured by heating for 15 min at 68°C in a solution containing 50% formamide (for transgene transcripts and host

 doi:10.20944/preprints201811.0606.v1

gene expression) or 50% urea (for siRNA derived from transgene transcripts, viroid-specific small RNAs, and miRNA), fractionated in 1.2% agarose gels containing 1×MOPS buffer at 50V for ~30 min (for transgene transcripts and host gene expression) or 12% polyacrylamide (acrylamide:bisacrylamide = 19:1) gels containing 1×TBE-8M urea at 450V for ~60 min (for siRNA derived from transgene transcripts, viroid-specific small RNAs, and miRNA), transferred to a nylon membrane (Biodyne), and hybridized with DIG-labeled cRNA probes for IR-DCL2/4 transcript, PSTVd, miR398a-3p (5'-TATGTTCTCAGGTCGCCCCTG-3'), and CCS1 (accession NM001347093) and SOD1 (accession NM001247102).

RT-qPCR analysis of endogenous DCL expression levels

Total RNA was extracted using TRizol reagent (Invitrogen, USA), and treated with TURBO DNA-free (Applied Biosystems, Ambion, USA). In accordance with the manufacturer's instructions, cDNA was synthesized from 1 μg RNA as a template using Superscript VILO (Invitrogen). qPCR analysis was performed essentially as described in Kasai et al. (2011) using SsoFastEvaGreen Supermix (Bio-Rad) with a Chrome4 real time PCR detector (Bio-Rad). Information used to design the PCR primers for tomato *DCL1*, *DCL2* (*DCL2a*), *DCL3*, and *DCL4* genes was obtained from the EMBL data base. The primers used for qPCR are described in Table S1.

sRNA preparation and deep sequencing analysis of PSTVd-derived sRNAs

Samples of leaf tissue (~1 g) were collected from line 72E and EC infected with PSTVd three wpi. Total RNAs extracted by TriReagent were quantified by UV spectrophotometry, and sent aliquots (ca. 2000 μg) to Hokkaido System Science Co., Ltd. (Sapporo, Japan) for small RNA sequence analysis (2Gb scale, paired end) on an Illumina HiSeq (Illumina, San Diego, CA, USA). Samples were quantified and their integrities verified using an Agilent 2100 Bioanalyzer (Agilent Technologies, Santa Clara, CA, USA), and processed using a TruSeq small RNA Library Prep Kit.

Adapter sequences were removed from the ends of the resulting raw short-read data based on the presence of an exact 10-nt match with the termini of the respective adapters, and identical short reads were grouped according to read size (15–45-nt). In this way, adapter-trimmed short read data was converted to a non-redundant "short-read-sequence occurrence" format. These non-redundant data were then mapped to either the genomic or anti-genomic strand of circular form of PSTVd genome using hssmap, a specially-written C language program to process the data.

MicroRNA analysis was performed manually using the latest miRBase (Release 21). A list of sequences that includes precursor miRNAs together with annotations for mature regions in microRNA was downloaded from miRBase (http://www.mirbase.org/).

ROS production and scavenging activity assay

The generation of ROS was analyzed by quantitating hydrogen peroxide using a commercial kit Radical catch (Hitachi Ltd., Tokyo, Japan). Briefly, a leaflet (ca. 0.2 g) was homogenized in 1 ml of 0.1 M sodium phosphate buffer (pH7.0) and centrifuged at 13,000 rpm for 5 min to collect supernatant. According to the manufacturer's instructions, an aliquot of the supernatant (10 μL) was mixed with a mixture of 5 mM of cobalt chloride solution (Reagent A; 25 μL) and luminol solution (Reagent B; 25 μL), and reacted for 120 seconds (s) to measure the amount of luminescence emission in an incubator (AccuFLEX Lumi400; Hitachi Ltd., Tokyo, Japan). Sample luminescence and the control luminescence was obtained by subtracting the measured value of 80 s from that of 120 s. Homogenization buffer was used for control. Statisctical analysis was performed using R software.

ROS scavenging activity was analyzed by quqntitqting hydrogen peroxide scavenging activity using the same kit. Briefly, the supernatant obtained above was further diluted 50-times with the same buffer. According to the manufacturer's instructions, an aliquot of the diluted supernatant (10 μL) was mixed with a mixture of 5 mM of cobalt chloride solution (Reagent A; 25 μL) and luminol solution (Reagent B; 25 μL), and incubated at 37°C for 5 min. The mixture was further added by hydrogen peroxide solution (1:1000-diluted Reagent C; 25 μL) and reacted for 120 s to measure the

 doi:10.20944/preprints201811.0606.v1

amount of luminescence emission. Sample luminescence and the control luminescence was obtained by subtracting the measured value of 80 s from that of 120 s. Homogenization buffer was used for control. Hydrogen peroxide scavenging activity was calculated using the following equation; i.e., Hydrogen peroxide scavenging activity (%) = {Luminescence (Control)-Luminescence (Sample)}/ Luminescence (Control) × 100. Statistical analysis was performed using R software.

RESULTS

Characterization of DCL2/4-knockdown transgenic tomato lines

The hairpin RNA produced by transcription of the SlartDCL2&4 IR transgene in tomato cells should activate the RNAi machinery, induce the production of siRNAs complementary to *DCL2* and *DCL4* transcripts, and suppress endogenous *DCL2* and *DCL4* expression. To assess the effects of transgene expression, we first verified the presence of transgene, transgene copy number, expression level of transgene transcript, and accumulation of siRNAs derived from transgene transcript in the three lines selected for study.

Presence of the transgene was examined by PCR amplification of CaMV-35S promoter sequence from genomic DNA extracted from transgenic lines. As a result, an amplicon of ~900 bp, the size expected from the primer set used, was detected from all the three lines of hpDCL2/4i (Figure S2a).

The transgene copy number was assayed by Southern-blot hybridization using a DIG-labeled cRNA probe for the CaMV-35S promoter. From line 51-6, two bands were detected in an *Eco*RI-digest and one band in the corresponding *Bam*HI digest, indicating that this line contains two copies. From line 72E, one band was detected in both the *Eco*RI and *Bam*HI digests, indicating that this line contains a single copy. Multiple (5–6) bands were detected in both the *Eco*RI and *Bam*HI digests of line 82a, indicating that this line contains multiple copies of the transgene (Figure S2b).

Transgene transcripts were assayed by northern hybridization using a DIG-labeled cRNA probe for SlartDCL2&4. A dense positive signal was detected from 1 μg of total RNA in line 72E, indicating the accumulation of high levels of transgene transcript. On the other hand, the signal was virtually invisible in samples from lines 82a and 51-6 as well as in the negative control line EC, even when higher amounts (10 μg) of total RNA were loaded (Figure S2c).

The level of siRNA accumulation derived from the transgene transcript was analyzed by northern-blot hybridization using the same probe as above. In lines containing the transgene, a positive signal with a size of ~20-nt was detected only in line 72E; no signals were visible for lines 51-6, 82a, and EC (Figure S2d).

DCL2/4-knockdown transgenic tomato line 72E developed severe disease symptoms upon PSTVd infection

Line 72E contains a single copy of the transgene and expresses high levels of transgene transcript and their corresponding siRNA. Therefore, changes in the appearance of line 72E plants in response to PSTVd infection were compared to those seen in other lines.

Ten plants each from lines EC and 51-6 showed very mild leaf curl four weeks after PSTVd inoculation and continued to grow, showing only slight growth retardation compared to the uninoculated healthy controls. In contrast, all ten plants of line 72E started to show curling on the newly expanding apical leaves two weeks post inoculation (wpi); this curling then became more severe, chlorosis appeared on the expanded leaves, and the mid-veins and/or petioles became necrotic around 3 wpi. The symptoms rapidly worsened between 3 – 4 wpi (Figure 1a, b and Figure S3).

Nine plants of line 82a (even though the expression of neither transgene transcript nor siRNA was evident) showed mild leaf curl and chlorosis at 3 wpi, symptoms that were milder than those on line 72E. Continued observation of infected line 72E plants revealed that growth almost stopped around 4 wpi, the severe necrosis first observed in the lower leaves became systemic, and, finally, the plants died three to four months post inoculation (Figure 1b). The infection assays were performed three times under the same conditions and the results were in agreement with those above.

Preprints (www.preprints.org) | NOT PEER-REVIEWED | Posted: 28 November 2018 doi:10.20944/preprints201811.0606.v1

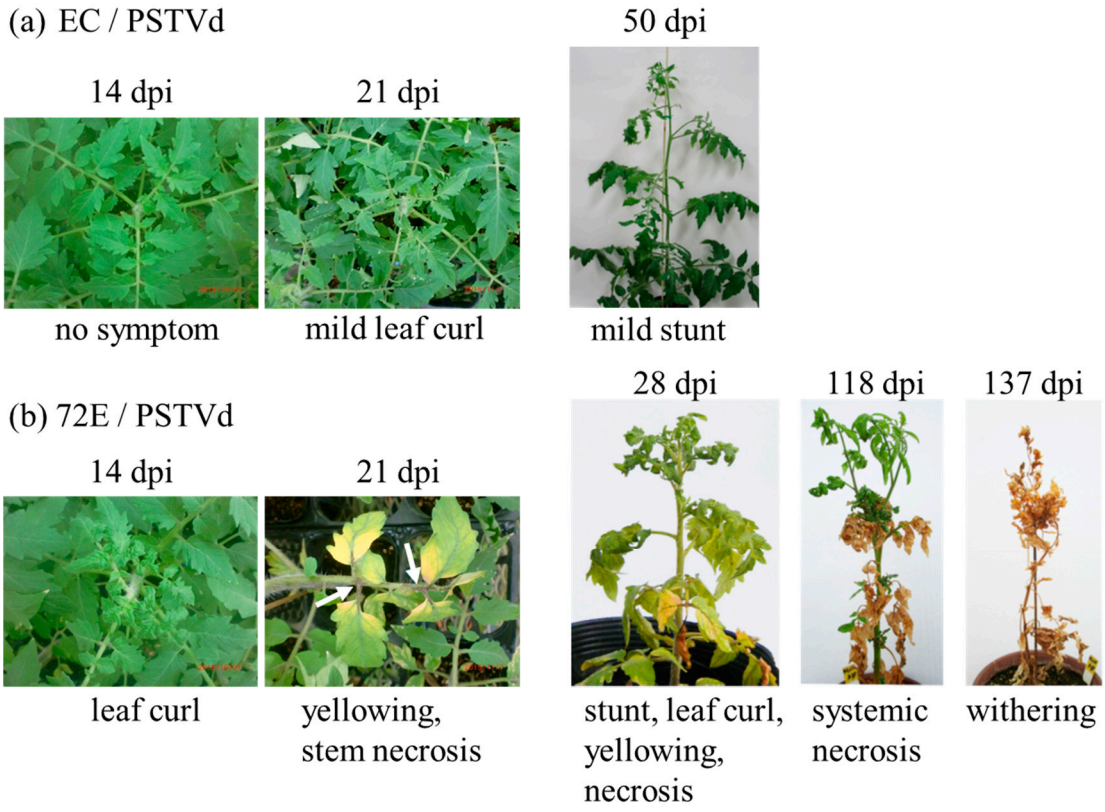

Figure 1. Lethal necrotic symptoms associated with PSTVd infection in the DCL2/4i-72E Moneymaker tomato line. The upper row indicates line EC infected with PSTVd. Plants showed mild leaf curling ~21 dpi and mild stunting at 50 dpi. The lower row indicates the 72E line infected with PSTVd. Infected plants started to show yellowing and stem necrosis around 3 – 4 weeks after inoculation, then showed severe systemic necrosis around 2–3 months post inoculation, and finally stopped growing and died. Three replicates of plants showed similar symptoms. Photos were taken on the days indicated above the pictures.

High levels of PSTVd accumulated in line 72E in the early stages and PSTVd differentially accumulated in transgenic lines

Total RNA extracted from the upper leaves of nine to ten individual tomato plants from each line at 2, 3, and 4 wpi was used to monitor the levels of PSTVd accumulation by northern-blot hybridization using a DIG-labeled PSTVd-cRNA probe. PSTVd was detected in almost every inoculated plant, even at 2 wpi (10/10 plants infected in line EC, 8/10 in line 51-6, 10/10 in line 72E, and 9/9 in line 82a. One or two weeks later, all plants were infected (Figure S4).

The intensity of the PSTVd-positive signal was visibly higher in line 72E compared to the other lines, especially at 2 and 3 wpi (Figure 2). Therefore, the intensities of each signal were quantified using the Quantity One software (BioRad), normalized by comparison with the signal intensities obtained with ethidium bromide staining, and then averaged per line per week. Finally, relative intensities were calculated by defining the average value of line EC at 2 wpi as 1.0. These calculations confirmed that relative accumulation levels were actually higher in line 72E early in infection: from high to low at 2 wpi, lines 72E (~2.1), EC (1.0), 82a (~0.75), and 51-6 (~0.7); at 3 wpi, lines 72E (~2.8), 82a (~2.1), EC (~1.9), and 51-6 (~1.45). Furthermore, although PSTVd concentrations in line 72E were twice as high as those in the other lines at 2 to 3 wpi, progeny levels were approximately the same later in the infection (lines 82a (~3.3), 72 E (~3.2), EC (~3.2), and 51-6 (~3.0) at 4 wpi).

 doi:10.20944/preprints201811.0606.v1

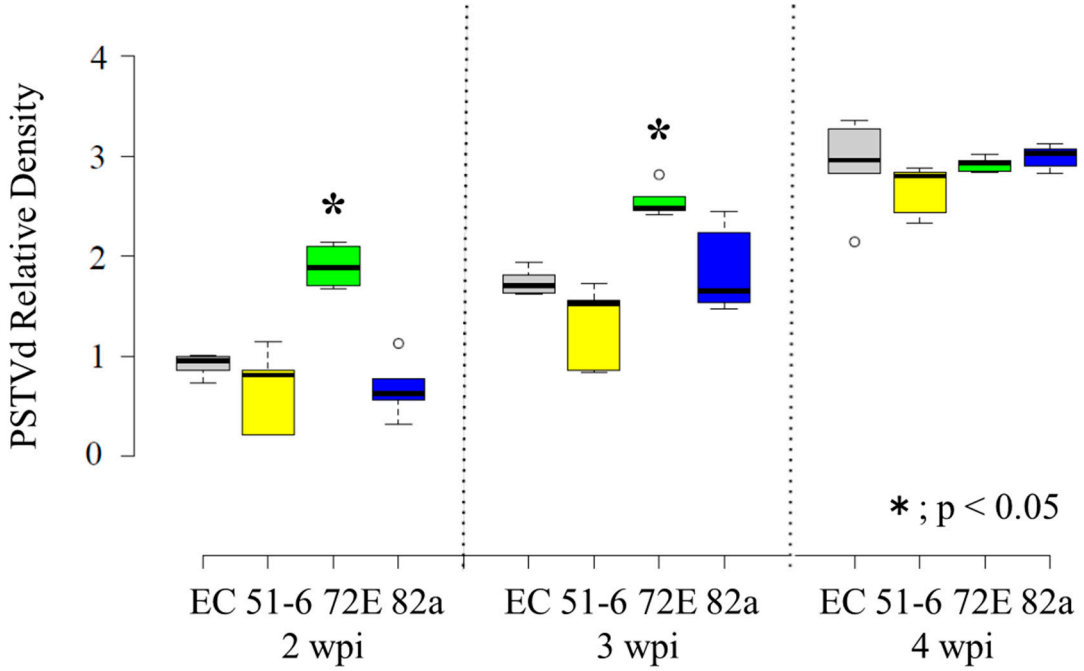

Figure 2. Relative density of PSTVd in three lines of DCL2/4i Moneymaker tomato and the empty casette control line at 2, 3, and 4 wpi. Five replicates of PSTVd-positive signals obtained by northern-blot hybridization were quantified by ChemiDoc XRS, normalized using the gel image stained with ethidium bromide, and the averages plotted on the graph. Thin vertical lines on the top indicate the error bar. The average value of the empty line at 2 wpi was adjusted as 1.0. The value in 72E line at 2 and 3 wpi with asterisks (*) were statistically significant at 5% level ($P < 0.05$). Boxplots were drawn in BoxplotR [77] using the Tukey whisker extent. Center lines show the medians; box limits indicate the 25th and 75th percentiles as determined by R software; whiskers extend 1.5 times the interquartile range from the 25th and 75th percentiles, outliers are represented by dots. n = 3 sample points.

PSTVd-sRNA of 21- and 22-nt species decreased and 24-nt species increased in the transgenic line 72E in response to knockdown of DCL2 and DCL4

In order to analyze the accumulation of PSTVd-derived sRNA (PSTVd-sRNA), groups of RNA extracts from nine to ten plants collected at weekly intervals were combined, aliquots (~10 μg) were fractionated by electrophoresis in an 8M-urea 12% polyacrylamide gel, transferred to nylon membrane, and hybridized with a DIG-labeled PSTVd-cRNA probe. Results revealed detectable levels of PSTVd-sRNA in lines EC and 72E even at 2 wpi; their size distributions were quite different, however. In the negative control line EC, the predominant species was 22-nt. In line 72E the major peak was two nucleotides longer (24-nt). This difference could be seen more clearly in the 3- and 4-week samples. Here, lines EC, 51-6, and 82a all accumulated abundant 22- and/or 21-nt species and a small amount of 24-nt species. Line 72E, in contrast, accumulated higher amounts of 24-nt species and trace levels of 21-nt species; the 22-nt species was virtually invisible in this sample (Figure 3). Note also that accumulation of PSTVd-sRNA increased in parallel with an increase in PSTVd genome RNA accumulation over 2 to 4 wpi.

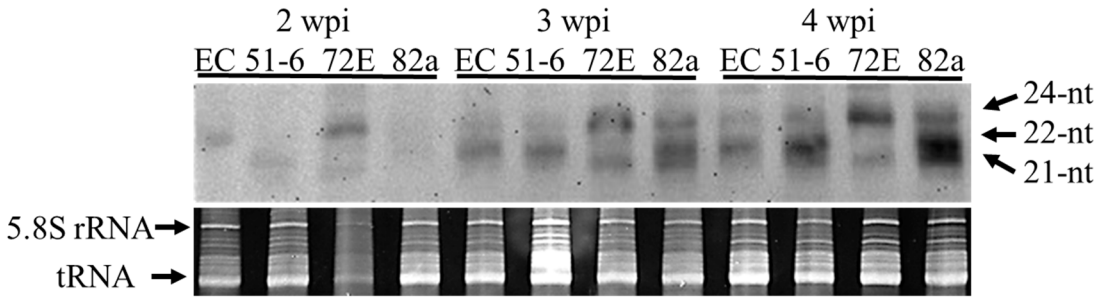

Figure 3. Time course analysis of PSTVd-sRNA accumulating in PSTVd-infected DCL2/4i-transgenic tomato lines. Total RNAs (~10 μg) extracted from three transgenic lines inoculated with PSTVd and the EC control at 2, 3, and 4 wpi were separated in 8M-urea 12% polyacrylamide gel, transferred to nylon membrane and analyzed by RNA gel-blot hybridization analysis using a DIG-PSTVd-cRNA probe. The upper panel shows the hybridization signal and the lower panel shows the loading control stained with ethidium bromide. All the lines except for 72E showed a dense hybridization signal at the position 22-nt and faint signals at 21- and 24-nt. In contrast, 72E line showed a dense signal at 24-nt and a faint signal at 21-nt. The signal at 22-nt was invisible.

The difference in the size distribution of PSTVd-sRNAs observed in line 72E is consistent with the suppression of *DCL2* and *DCL4* expression by RNAi in the line. That is, the decrease in 21-nt species can be explained by down-regulation of *DCL4* which is responsible for producing 21-nt sRNAs. Similarly, the decrease in 22-nt species is consistent with down-regulation of *DCL2* responsible for production of 22-nt species. It should be noted here that the observed decrease in 21-nt species was not as pronounced as that in 22-nt species.

PSTVd infection activates DCLs

The levels of *DCL1*, *DCL2*, *DCL3* and *DCL4* transcripts before and after PSTVd infection in line 72E were analyzed by RT-qPCR (Figure 4). Before PSTVd infection, the levels of *DCL2* and *DCL4* transcripts in healthy line 72E plants were significantly lower ($P < 0.05$) than those in the healthy line EC plants. In contrast, levels of *DCL1* transcripts were almost identical, and levels of *DCL3* transcripts were slightly (but not significantly) lower in line 72E. This result, as expected, indicated that expression of the *DCL2* and *DCL4* genes had been down-regulated in line 72E by RNAi before PSTVd infection. In contrast, transcript levels of *DCL1*, *2*, *3*, and *4* were all significantly up-regulated in line 72E after PSTVd infection. The increase in *DCL1* was especially remarkable ($P < 0.01$). This was also true for line EC, indicating that transcription of *DCL1–4* was activated by PSTVd infection but that changes were somewhat bigger in line 72E than in line EC.

Preprints (www.preprints.org) | NOT PEER-REVIEWED | Posted: 28 November 2018 doi:10.20944/preprints201811.0606.v1

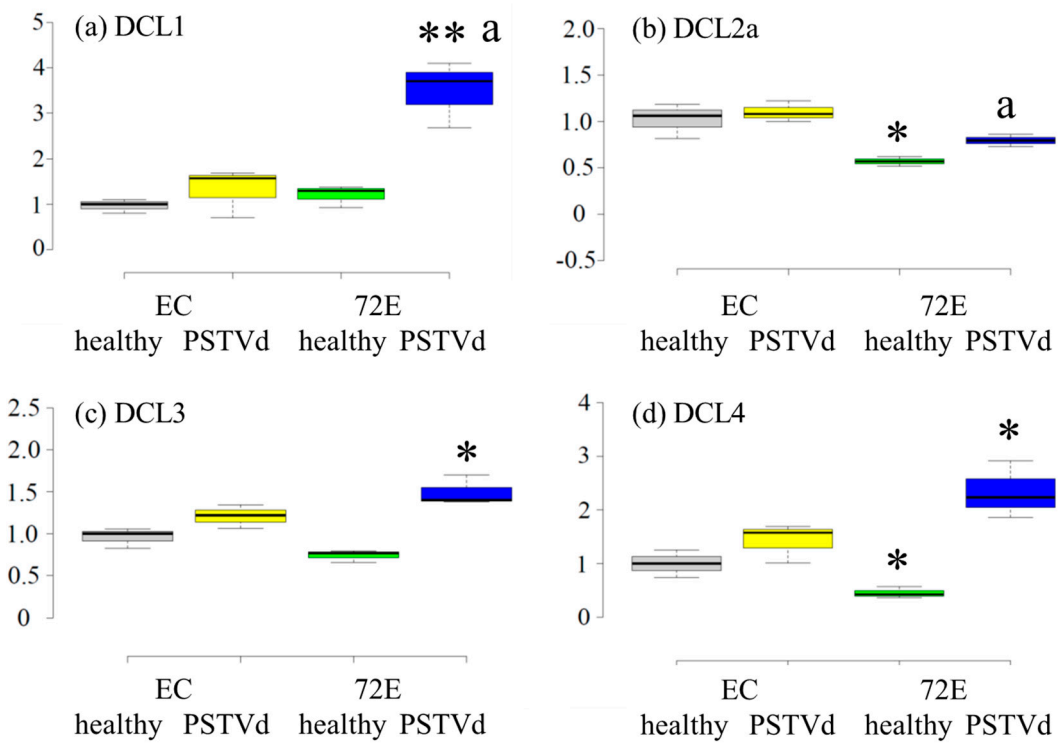

Figure 4. RT-qPCR analysis of endogenous *DCL1*, *2*, *3*, and *4* mRNAs in 72E and empty casette lines with or without infection of PSTVd. Levels of *DCL2* and *4* mRNAs in 72E line were significantly low compared to those in the empty casette before PSTVd infection, suggesting that endogenous *DCL2* and *4* mRNAs were successfully down-regulated in the 72E line. Levels of mRNAs of *DCL1*, *3* and *4* were significantly up-regulated in 72E line by PSTVd infection. Surprisingly, *DCL2* was also up-regulated in the 72E line compared to the healthy line, suggesting that expression of tomato *DCL* genes are significantly activated by PSTVd infection. The value with double asterisk (**; $P < 0.01$) and single asterisk (*; $P < 0.05$) were statisctically significant at 1% and 5% level compared to healthy EC line. The value with "a" (a; $P < 0.05$) were statistically significant at 5% level compared to PSTVd EC line.

The level of *DCL1*, *2*, *3*, and *4* transcripts before and after PSTVd infection was also examined by northern-blot hybridization, but most of all the levels were below the detection limit, except that faint signals were observed after PSTVd infection in lines 72E and EC.

Deep sequencing analysis of sRNAs from line 72E

It is generally believed that vd-sRNA processed by multiple DCLs activities after induction of RNA silencing may play a major role in viroid pathogenesis or symptom expression. Thus, we carried out deep sequencing analysis of sRNAs prepared from PSTVd-72E and compared the changes in PSTVd-sRNA, host miRNAs, and the other sRNAs with those observed in PSTVd-EC. The sRNA data sets obtained by Illmina Hiseq small RNA analysis contained a total 23,604,108 reads ranging in size from 15–45-nt in PSTVd-72E sampled at 3 wpi and 23,864,986 reads in the comparable sample from PSTVd-EC.

Overview of the changes in PSTVd-sRNA reads between PSTVd-72E and PSTVd-EC preparations: Allowing a maximum of 1-nt mismatch, PSTVd-sRNA sequences accounted for 678,643 reads in PSTVd-72E and 554,261 reads in PSTVd-EC samples. PSTVd-sRNAs in PSTVd-72E comprised 383,947 reads (69%) from plus-strand and 170,091 reads (31%) from the minus-strand. i.e., sRNAs derived from the plus-strand were slightly more than twice as abundant as those from the minus-strand (Figure S5 and S6). This ratio was very similar in line EC; i.e., 318,585 reads (63%) to 188,092 reads (37%).

Preprints (www.preprints.org) | NOT PEER-REVIEWED | Posted: 28 November 2018 doi:10.20944/preprints201811.0606.v1

In contrast, and as expected from the data obtained by RNA gel-blot hybridization, the size distributions of PSTVd-sRNAs in these two lines were quite different. In line EC, the most abundant size class was 22-nt (50%), followed by 21-nt (36%), 24-nt (5%), and 23-nt (5%), a result which corresponded to our previous data obtained from PSTVd-infected Rutgers tomato [9, 64]. In PSTVd-72E, however, the most abundant size class was 24-nt (53%), followed by 21-nt (23%), 17-nt (18%), 23-nt (4%), and 22-nt (3%) (Figure 5a and b). These results were quite consistent with the data obtained by RNA-gel blot assay described above. That is, by knocking down *DCL2* and *DCL4* expression using an RNAi strategy, the number of PSTVd-sRNA reads containing 22-nt in PSTVd-72E dropped sharply to levels about one-twentieth of those seen in line EC plants (i.e., from 253,425 reads in PSTVd-EC to 14,257 in PSTVd-72E), but the number in the 24-nt class increased approximately 10-fold (i.e., from 27,255 reads in PSTVd-EC to 295,542 reads in PSTVd-72E). The number in the 21-nt class also decreased in PSTVd-72E, but this decline was much smaller than in the 22-nt class, even though expression of *DCL4* as well as *DCL2* was knocked down, suggesting that *DCL1*, in addition to *DCL4*, plays an important role in the production of 21-nt PSTVd-sRNA (see Discussion session).

(a) EC-PSTVd

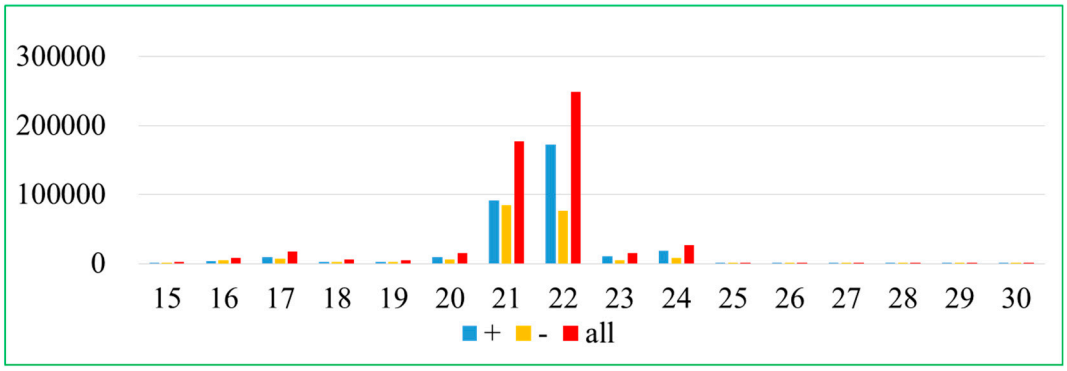

(b) 72E-PSTVd

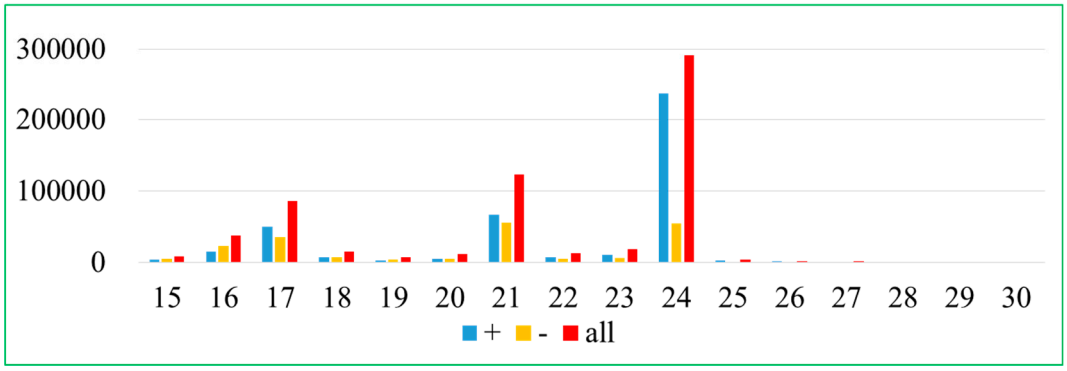

Preprints (www.preprints.org) | NOT PEER-REVIEWED | Posted: 28 November 2018 doi:10.20944/preprints201811.0606.v1

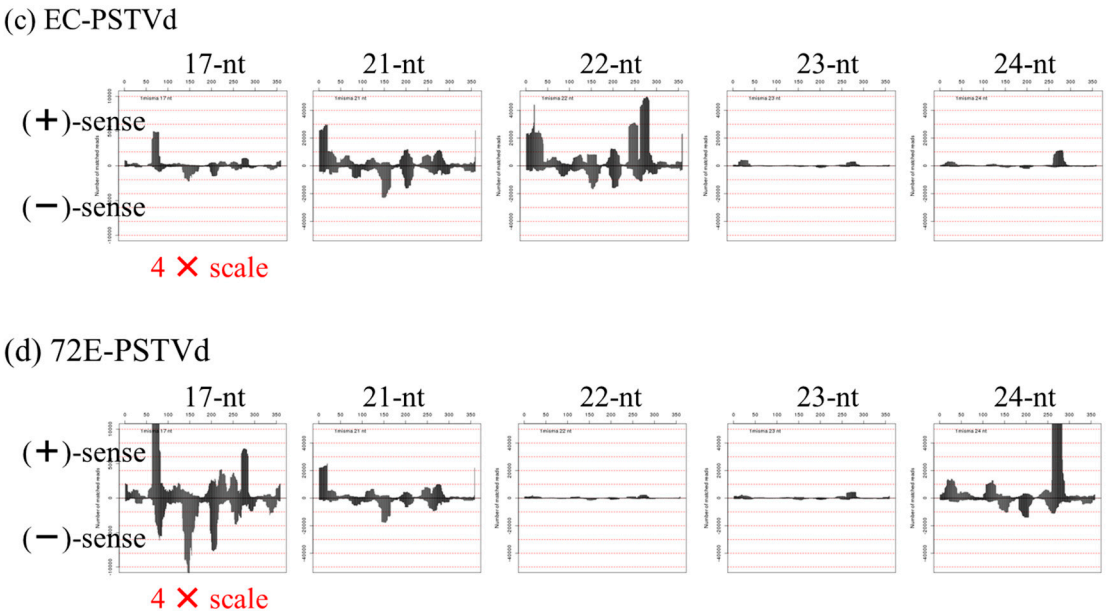

Figure 5. Size distribution and positive (+) / negative (–) ratio of PSTVd-sRNAs of the size 15–30-nt accumulated in the (a) EC and (b) 72E lines. Panels c and d compare the PSTVd-sRNA hotspot patterns for the 17-nt, 21-nt, 22-nt, 23-nt, and 24-nt species in the EC (c) and 72E (d).

Interestingly, molecules in the 17-nt class accounted for 18% of the total PSTVd-sRNA reads and were ranked the third most abundant class in PSTVd-72E. At present, it is not clear why the 17-nt class increased so extensively in line 72E, and the possible function of the 17-nt class has yet to be determined. It should be noted here that the majority of these molecules originate from the upper portion of the pathogenicity region; furthermore, the most abundant member of this class, which accounted for 17,606 reads (~19.2%) corresponds to nucleotides 63–79 in the PSTVd genome (5′-AGGCGGCTCGGAGGAGC-3′).

Although the size distributions of PSTVd-sRNA were quite different for PSTVd-72E and PSTVd-EC, the hotspot patterns were virtually identical. This was most evident for the 21-nt species in which the total numbers of reads for the two lines were not significantly different (Figure 5c and d). Interestingly, this was also the case for the 22-nt and-24 nt species where the total numbers of PSTVd-sRNA reads were significantly different; i.e., it was clear that the hotspot patterns of PSTVd-sRNAs in PSTVd-72E and PSTVd-EC were virtually identical when the scales of vertical axis were normalized.

Note also that the hotspot patterns seen in this analysis were very similar to those from PSTVd-infected Rutgers tomato presented in our earlier report [11], indicating a high degree of reproducibility among multiple deep sequencing analyses (Figure S7). The fact that the hotspot pattern of PSTVd-sRNA remained constant even when the size distribution changed substantially suggested that even a significant change in the hierarchical order of DCL function caused by RNAi-mediated down-regulation of *DCL2* and *DCL4* expression was not sufficient to change the potential recognition sites and cleavage activities of the individual DCLs.

Changes in host sRNAs and miRNA expression levels in PSTVd-72E and –EC – PSTVd infection up-regulated miR398 and miR398a-3p: In PSTVd-72E, expression levels of all four *DCL*s were altered, and, as a result, the size distribution of PSTVd-sRNA changed extensively. Also, because the overall response to PSTVd infection in line 72E changed from tolerance to high sensitivity, relative levels of miRNAs and other host-derived sRNA species in this line were compared with those in PSTVd-EC plants. As described above, these comparisons were made using 21-nt species in which the total number of reads did not change so much between lines 72E and EC. After normalization to the ratio per million reads, comparison of all sRNAs present at levels more than 50 reads per million revealed that 12 species of miRNAs were up- or down-regulated by more than three times in PSTVd-72E. The

Preprints (www.preprints.org) | NOT PEER-REVIEWED | Posted: 28 November 2018 doi:10.20944/preprints201811.0606.v1

data presented in Table 1 reveals that nine species of miRNAs were up-regulated, whereas three species were down-regulated. In particular, miR398 and miR398a-3p showed unusually high expression levels in PSTVd-72E, where the number of reads per million increased from 311 to 2,080 and from 1,922 to 16,676, respectively. As described below, these miRNAs are known to target the mRNA of superoxide dismutase which removes harmful ROS from the cell.

Table 1. Changes in tomato sRNA levels in lines PSTVd-72E and -EC.

Name small RNA	Empty casette		72E	
	rank	reads*1	rank	reads*1
Top 5				
miR166d-3p	1	176745	1	190257
25S rRNA (LOC108175346)	2	89566	2	133774
miR159a	3	31728	3	45000
miR166c	4	30583	5	21196
miR396b	5	26599	4	27205
micro RNA				
miR398a-3p*	41	1922	8	16676
miR398*	263	311	39	2035
miR166	31	2260	30	8450
miR171e	1578	33	374	184
miR393-3p	1098	52	259	275
miR397-5p	437	176	101	769
miR408b-3p	151	528	40	1996
miR4376-5p	54	1417	18	4375
miR1919-3p	1037	57	411	159
miR166b	13	7386	30	2500
miR399i-3p	401	152	1432	29
miR477-5p	878	71	2274	15
ribosomal RNA				
25S rRNA (LOC108175346)	10	8109	721	76
25S rRNA (LOC108175346)	17	3893	1355	32
25S rRNA (LOC108175346)	20	2970	1224	37
25S rRNA (LOC108175346)	27	2623	494	130
25S rRNA (LOC108175346)	28	2595	811	68
25S rRNA (LOC108175346)	45	1739	15448	2
Dicer-related				
DCL2d	11234	2	14	7596
DCL4	48061	1	15	6696
DCL2	—	0	16	5781
DCL2c	—	0	19	4014
DCL2 (LOC102580326)	—	0	24	3173
DCL2 (LOC102580979)	—	0	25	3145
DCL4	—	0	32	2448
DCL2a	—	0	33	2401
DCL2a	—	0	34	2213
DCL4	—	0	35	2109
DCL2a	—	0	42	1919
DCL2a	—	0	45	1775
PHAS				
Sly-PHAS16 precursor siRNA	19	3158	2426	14
Sly-PHAS04	49	1545	54902	1
others				
uncharacterized ncRNA (LOC101245085)	15	4564	—	0
DNA-directed RNA polymerase III subunit 1	21	2968	177	414
Solanum lycopersicum chromosome 1	151	451	40	1996
probable indole-3-pyruvate monooxygenase	44	1749	1520	22

*miR398 and miR398a-3p were up-regulated 770–868 % in the 21-nt sRNA population from PSTVd-72E compared to those from PSTVd-EC. miR398 has been reported to target Cu/Zn dismutases (CSD1 and CSD2)

 doi:10.20944/preprints201811.0606.v1

in *Arabidopsis spp.* miR398a-3p has been reported to direct the cleavage and/or translational repression of CCS1 mRNA in *Arabidopsis spp.* and possibly in tomato. Levels of miR166C-3p in line PSTVd-72E were only half those found in PSTVd-EC.

As shown in Table 1, several sRNAs of host origin, other than miRNA species, were also detected. Some of these greatly fluctuated in the number of reads in PSTVd-72E but the others did not fluctuate (Table 1). The top five (i.e., miR166b, 25S rRNA (LOC108175346), miR159a precursor RNA, miR166c, and miR396b) were almost the same in order; i.e., a difference was only seen in the order of the 4th and 5th places. Interestingly, 12 of the top 50 sRNAs in PSTVd-72E were those derived from *DCL2* (9 species with 7,596–1,775 reads/million) and *DCL4* (3 species with 6,845–2,019 reads/million); however, they were approximately zero in PSTVd-EC. Therefore, it was confirmed that RNAi-mediated digestion of transgene-derived and/or endogenous transcripts of *DCL2* and *DCL4* genes actually took place in line 72E plants.

In addition, it should be noted here that five species of 21-nt sRNAs derived from 25S rRNA decreased in number extensively from 8,109–1,739 to 130–37, Sly-PHAS 16 precursor siRNA decreased from 3,158 to 14, and Sly-PHAS04 precursor siRNA decreased from 1,545 to 1.

Nucleotide sequence of the progenies propagated in line 72E was the same as that in line EC: The complete nucleotide sequences of PSTVd progenies propagated in lines 72E and EC was examined by using cDNA clone-sequencing (10 each of cDNA clones) and by analysis using the deep sequencing data of PSTVd-sRNAs as described by Suzuki et al. [65], and found that they were virtually identical to the original sequence infected, although some minor singleton mutations, probably raised by replication error or misincorporation during PCR, were detected.

Northern-blot hybridization of miR398a-3p in healthy and PSTVd-infected lines 72E and EC – PSTVd infection up-regulated miR398a-3p

Changes in miR398a-3p expression levels after PSTVd infection were also examined by northern-blot hybridization. Aliquots (10 μg) of total RNA, extracted from healthy and PSTVd-infected lines 72E and EC, were fractionated by 8M-urea 12% polyacrylamide gel electrophoresis, transferred to a nylon membrane, and hybridized with a DIG-labeled cRNA probe for miR398a-3p. As shown in Figures 6A and 6B, miR398a-3p was not detectable in healthy plants from either line, indicating that expression levels of miR398a-3p were very low. In contrast, in PSTVd-infected plants, miR398a-3p reached detectable levels at 3 wpi (Figure 6b, arrow), indicating that PSTVd infection stimulates expression of miR398a-3p. In agreement with the deep sequencing data, the level of miR398a-3p in PSTVd-72E was ~5 times higher than that in the comparable PSTVd-EC plants, reconfirming that RNAi-mediated down-regulation of *DCL2* and *DCL4* results in enhanced expression. This analysis was repeated twice and yielded similar results.

 doi:10.20944/preprints201811.0606.v1

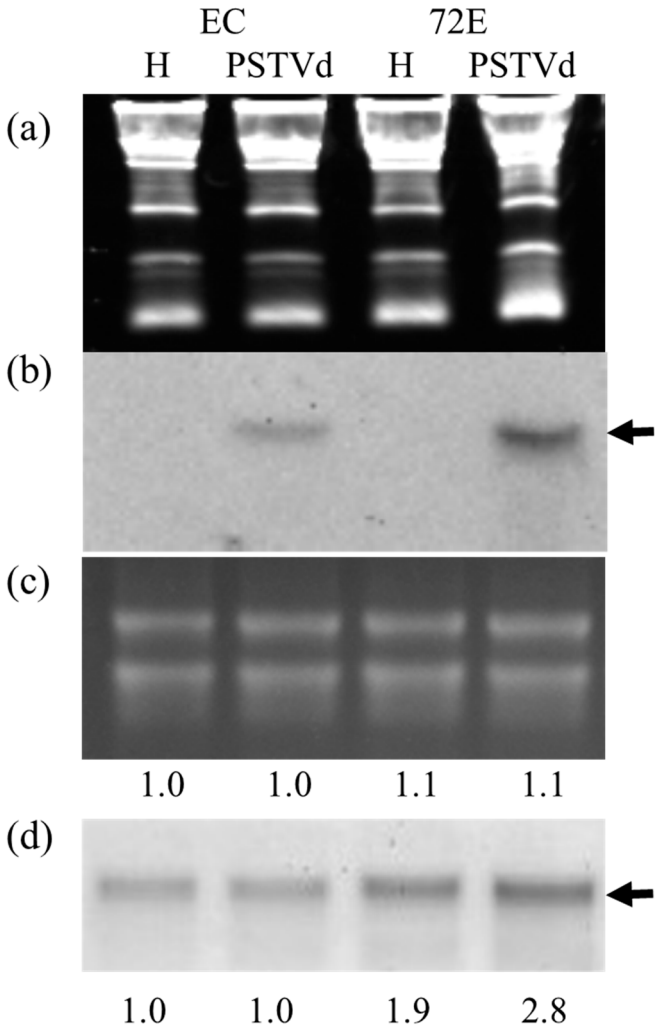

Figure 6. Northern-blot hybridization of miR398a-3p (panel (a) and (b)) and SOD1 (panel (c) and (d)). Aliquots (10 μg) of total RNA, isolated at 3 wpi, were fractionated by electrophoresis in 8M-urea 12% PAGE, transferred to nylon membrane, and hybridized with a DIG-labeled cRNA probe for miR398a-3p and SOD1. Band signals were visualized by ChemiDoc XAR (BioRad) and quantified with Quantity One software (Bio-Rad). miR398a-3p was detectable only after PSTVd infection, and signal intensities were ~2.5–5.0 times higher in line 72E as compared to a control line EC. This analysis was repeated twice. SOD1 was detected from all samples, and the level of expression was especially enhanced in PSTVd-72E.

Expression of tomato SOD1 and CCS1 in healthy and PSTVd-infected lines 72E and EC

Because miR398a-3p is reported to target CCS1 mRNA in tomato [61], which, in concert with cytosolic SOD1, has a function to control detoxification of harmful ROS in the cell, changes in the expression level of *SOD1* and *CCS1* genes following PSTVd infection was analyzed by northern-blot hybridization. Aliquots (2 to 10 μg) of total RNA, extracted from healthy and PSTVd-infected lines 72E and EC at 3 wpi, were fractionated by 1.2% agarose gel electrophoresis as described above and hybridized with DIG-labeled cRNA probes for *SOD1* and *CCS1*.

SOD1 transcripts were readily detected from 2 μg of total RNA preparations from all samples, indicating relatively high levels of expression of the gene. Among them, line 72E, and particularly PSTVd-72E, showed a higher expression level than line EC. The relative expression level was 1.0, 1.0, 1.7 and 2.5 for healthy-EC, PSTVd-EC, healthy-72E, and PSTVd-72E, respectively (Figure 6c, d and Figure. S8). The results revealed that transcription of *SOD1* was particularly activated in line 72E by PSTVd infection. On the other hand, *CCS1* transcript was not detected constantly, even from ~10 μg

Preprints (www.preprints.org) | NOT PEER-REVIEWED | Posted: 28 November 2018 doi:10.20944/preprints201811.0606.v1

of total RNAs, suggesting that the expression level was low. The analysis was repeated three times with very similar results.

ROS production and acavenging activity in PSTVd-infected line 72E plant

Hydrogen peroxide, one of ROS, activity was assayed in the healthy and PSTVd-infected lines 72E and EC during the period from 4–10 wpi, because in the meantime, PSTVd-72E stopped growing and severe necrosis symptoms were underdeveloped. Leaf 5 (lower) and a mixture of leaf 7 and 8 (upper) were selected for the analysis, because PSTVd-infected line 72E plant started to show leaf yellowing and petiole necrosis in leaf 5 and 6 around 4 wpi, but showed only leaf curing in leaf 7 and the uppers. The assay was repeated twice, and each analysis consisted of three biological replicates collected randomly from five plants per treatment. The highest activity was observed in leaf 5 of PSTVd-72E. Interestingly, the activity was also high in leaf 5 of healthy-72E. Average hydorogen peroxide activity in leaf 5 was ca. 15 and 5 times higher in PSTVd-72E and in healthy 72E than in healcthy-EC and PSTVd-EC. Statisctically valuable difference ($p<0.01$) was found between healthy-EC and healthy- and PSTVd-72E (Figure 7a; Table S2). In contrast, the activity was equally low in every samples in 7–8 leaf, indicating that the lower leaves of PSTVd-72E plant shows higher levels of hydrogen peroxide activity.

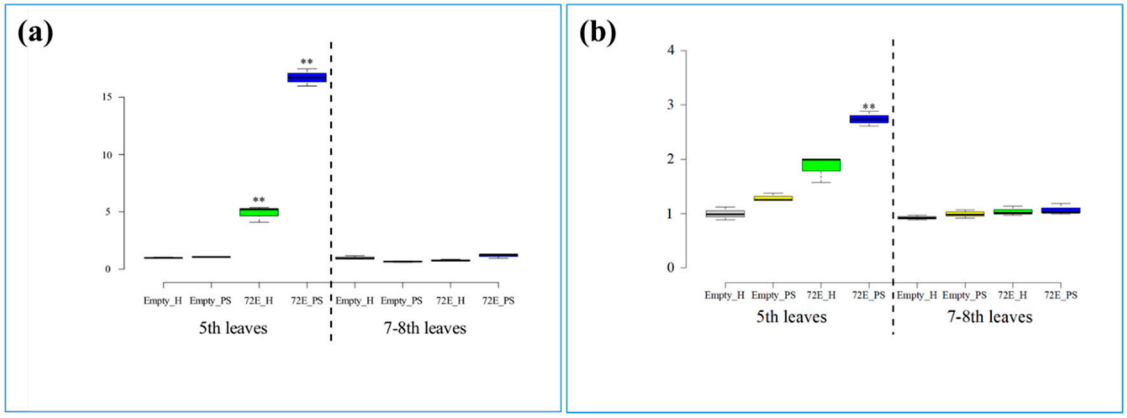

Figure 7. Relative ROS production (a) and relative ROS scavenging activity (b) of the 5th and 7–8th true leaves. Center lines show the medians; box limits indicate the 25th and 75th percentiles as determined by R software; whiskers extend 1.5 times the interquartile range from the 25th and 75th percentiles, outliers are represented by dots. n = 3 sample points.

Hydrogen peroxide, one of ROS, scavenging activity was also assayed similarly in leaf 5 and leaf 7–8 in the healthy and PSTVd-infected lines 72E and EC. Average hydorogen peroxide scavenging activity was 20% in healcthy-EC, 27.5% in PSTVd-EC, 33.6% in healthy-72E, and 44% in PSTVd-72E. Statisctically valuable difference ($p<0.01$) was found between healthy-EC and PSTVd-72E (Figure 7b, Table S2), indicating that the lower leaves of PSTVd-72E plant shows higher levels of hydrogen peroxide scavenging activity.

Discussion

In this experiment, by using RNAi-mediated matter, we produced a T3-generation of DCL2&4-knockdown Moneymaker tomato lines, transformed with an IR construct consisting of partial sequences of tomato homologs *DCL2* and *DCL4*. One of these lines, named line 72E, was shown to contain a single copy of the transgene and to express high levels of transgene transcript and related siRNAs.

Line 72E, when challenged by PSTVd inoculation, started to show apical leaf curl at approximately 2 wpi and exhibited systemic leaf chlorosis, accompanied by vein necrosis at 3 to 4 wpi. The plants subsequently stopped growing, developed more severe leaf necrosis (from lower to systemic), and finally died 4 to 5 months after inoculation, suffering from lethal systemic necrosis.

 doi:10.20944/preprints201811.0606.v1

This was in contrast to line EC, which was used as a control. Since Moneymaker tomato is a tolerant cultivar to PSTVd infection [10, 66], line EC showed very mild leaf curl and stunting during the observation period. Therefore, RNAi-mediated down-regulation of *DCL2* and *DCL4* expression changed Moneymaker tomato into being highly susceptible to PSTVd infection.

In line with the severity of disease symptoms, PSTVd level was significantly higher (1.5 to 3.0 times) in line 72E than in the other lines in early infection (until 2 and 3 wpi) (Figure 2), indicating that DCL2 and DCL4 play an important role in protecting tomato plants from PSTVd-induced symptom expression by suppressing the initial replication and accumulation of PSTVd.

By the analysis of PSTVd-sRNA using RNA-gel blot assay, lines EC, 51-3 and 82a were found to have accumulated two major bands of the sizes 21- and 22-nt and a weak band of 24-nt, whereas line 72E accumulated a dense 24-nt band and faint 21-nt band. The result was more evident in the data after deep sequencing: the number of PSTVd-sRNA reads of the sizes 21- and 22-nt species in line 72E decreased to ~66.7% and ~5% of those in line EC, respectively, and the 24-nt species in line 72E increased by ~1100% that in line EC.

Considering the commonly accepted concept that DCL1, DCL2, DCL3, and DCL4 generate 21-nt, 22-nt, 24-nt, and 21-nt sRNAs, respectively, the result clearly indicated that RNAi-mediated down-regulation of *DCL2* and *DCL4* resulted in the decrease of 21- and 22-nt species; 24-nt species, in contrast, increased significantly by relative superiority of DCL3 activity. The result is in line with the previous findings on the changes in the size distribution of virus- and viroid-derived sRNAs accumulated in *dcl2* and *dcl4* mutants and/or the knockdown lines [20, 21, 50, 58, 60]. The underlying mechanism behind this is hierarchical interaction existing in the functions of DCLs in antiviral defense; i.e., DCL4 preferentially plays a major role in general. However, DCL2 is known to compensate for DCL4 function once DCL4 is destroyed or interfered [50, 58, 60]. Similarly, Katsarou et al [21] reported, by using PSTVd-infected *dcl*(s) mutant lines of *Nicotiana benthamiana*, that the combined activity of DCL2 and DCL3 is important for anti-viroid defense. They presented a model that shows that DCL4 normally plays a major role in anti-viroid defense and suppresses the functions of DCL2 and DCL3. This was also the case in our experiment on the PSTVd-infected tomato hpDCL2/4i-72E line, in which the activity of DCL3 was significantly enhanced when expression of *DCL2* and *DCL4* was artificially suppressed.

Another dramatic increase found in 17-nt species in the 72E line was particularly interesting because a majority of them were originated from the upper strand of the pathogenicity region. The biogenesis is unknown, but a similar mechanism, reported by Zhu et al [67], may be included, in which bidirectional processing of pri-miRNAs with branched terminal loops by *Arabidopsis spp.* Dicer-like1 results in production of 16–17-nt species, because viroids can form branched terminal loop structures and DCL1 was active in the plants.

As described above, RNAi-mediated knockdown of *DCL2* and *DCL4* created a significant change in the size distribution of PSTVd-sRNAs. Nevertheless, the rate of decrease in 21-nt species (~33%) was apparently smaller than that in 22-nt species (~95%). This big difference seems to contradict the data obtained by RT-qPCR on the expression of all four *DCLs*; namely, the rate of decrease in *DCL2* and *DCL4* expression in 72E line was ~50–60% of the empty casette, not so different from each other. Taking the result that the rate of decrease in the transcription level of *DCL4* (producing 21-nt species) was almost the same as that of *DCL2* (produces 22-nt species), and also the fact that DCL1 is also responsible for producing 21-nt species, the results may indicate that DCL1 is actually involved in the processing of viroid RNA and contributes to the production of 21-nt species of vd-sRNA, as suggested previously [68, 69].

RT-qPCR analysis clearly indicated that PSTVd infection activated transcription level of *DCL4* in line 72E. On the other hand, the activation of transcription by PSTVd infection was observed not only in *DCL4* but also the other *DCLs* including *DCL2*, indicating that expression of all the *DCLs* was activated by PSTVd infection. Since it was reported that the levels of *DCL1*, *DCL2*, and especially *DCL4* transcripts were increased significantly in a wild type tomato (cv. Rutgers) by the infection of citrus exocortis viroid (CEVd), another member of the genus *Pospiviroid* [70], it may be a general phenomenon for viroids, at least those in the genus *Pospiviroid*.

An important point here is that the sensitivity to PSTVd infection largely changed in line 72E, even though all the *DCLs* expression levels seemed to increase or somewhat recover after PSTVd infection. The result seems to create a question that cannot be explained by the expression levels of individual *DCLs*. An appropriate balanced expression of all the *DCLs* may be important to express an optimum anti-viroid defense response. Further analysis on the activities of DCL enzymes, for example, is necessary to clarify this point.

By *in silico* analysis of changes in miRNA reads in the sRNA deep sequencing data, several miRNAs were found to have been up- or down-regulated in PSTVd-72E, compared to PSTVd-EC. Among them, the increased number of miR398 (770%), and especially miR398a-3p (868%), in PSTVd-72E was extremely interesting. miR398 and miR398a-3p are stress-induced miRNAs known to be expressed in response to various stresses and inhibit the expression of cytosolic and chloroplast-localized superoxide dismutases [71, 72] and target mRNAs encoding CCS1, which deliver copper to SOD apoproteins in different cellular compartments [61]. In fact, northern-blot hybridization analysis clearly showed that miR398a-3p was detected exclusively from PSTVd-infected plants (i.e., both of 72E and EC) and the intensity of the band was ~5 times higher in PSTVd-72E than in PSTVd-EC. Parallel to this, SOD1 expression was also activated by PSTVd infection, especially in PSTVd-72E.

Because miR398a-3p (and/or 398) and SOD1, in concert with CCS1, control the detoxification of harmful ROS in the cell, the results, along with the observation that PSTVd-72E caused severe systemic necrosis, strongly support that ROS is generated not only in PSTVd-72E but also in PSTVd-EC. Since PSTVd-EC, as well as healthy-72E and -EC, showed no visible necrotic symptoms at all, unusually higher levels of ROS production in PSTVd-72E, which is supported by enhanced up-regulation of miR398a-3p and miR398, seemed to be a major reason for the development of severe necrotic reaction. In fact, analysis of ROS production and scavenging activity during the period when plant developed symptoms (leaf curl and yollowing) and stopped growing but severe necrosis symptoms were underdeveloped, it was revealed that both of ROS production and scavenging acitivities were high in PTVd-72E, showing that ROS is generated actively and in the meantime acavenged desperatively in the plant. PSTVd-sensitive tomato cultivars such as Rutgers often develop various degrees of leaf and/or vein necrosis, especially by infection of severe and lethal strains of PSTVd, CEVd, and tomato apical stunt viroid [73, 74]. The observations presented here are probably a general phenomenon underlying PSTVd–tomato interactions. Recent data from comprehensive and global transcriptome and metabolome analyses suggested that viroid infection triggers a plant immune response and results in activation of various signaling pathways and associated activities such as MAPK3, PR1, 1,3-beta-glucanase, and ROS biogenesis [10, 66, 75, 76]. Our results strongly support this notion.

In conclusion, the results presented here clearly indicate that tomato homologs of *DCL2* and *DCL4* provide strong but incomplete anti-viroid defense and suppress viroid accumulation early in infection. Replication of highly-structured dsRNA-like hairpin RNA from the viroid genome serves as a PAMP and activates the RNA-silencing targeting viroid, which can be regarded as PAMP-triggered immunity. As a result of this innate immunity, PSTVd-tolerant tomato cultivars like Moneymaker continue to grow almost normally and show very few disease symptoms. Even in this case, however, our results indicated that SOD1 and miR398/miR398a-3p is activated in the plant, indicating that another defense reaction accompanying ROS production is activated by continuous replication/accumulation of viroid RNA resistant to RNA silencing [18]. In contrast, hpDCL2/4i-Moneymaker tomato line fails to defend initial viroid infection by RNA silencing, and as a result, allows more aggressive replication/accumulation of viroid, which seems to trigger excessive production of ROS that is not controlled by SODs, in concert with CCS1 and miR398/miR398a-3p, and results in the development of severe systemic necrosis, leading to plant death.

Acknowledgments: We thank Dr. Robert A Owens (USDA/ARS, MPPL, USA) for critical reading and valuable suggestions on the manuscript.

Funding information: This study was supported in part by Japan Society for the Promotion of Science (JSPS) KAKENHI grant no. 15H04455 and 18H0221 to T.S.

Conflicts of interest: The funders of this work had no role in study design, data collection and analysis, decision to publish, or preparation of the manuscript.

References

1. 1. Diner, T.O. Potato spindle tuber "virus": IV. A replicating, low molecular weight RNA. *Virology.* **1971**, 45:411–428.
2. 2. Di Serio, F.; Flores, R.; Verhoeven, J.T.J.; Li, S.-F.; Pallás, V.; Randles, W.J.; Sano, T.; Vidalakis, G.; Owens, R.A. Current status of viroid taxonomy. *Arch. Virol.* **2014**, 159, 3467–3478.
3. 3. Ding, B.; Wang, Y. Viroids: uniquely simple and tractable models to elucidate regu-lation of cell-to-cell trafficking of RNAs. *DNA Cell Biol.* **2009**, 28:51–56.
4. 4. Diener, T.O. Biological properties. In *The Viroids*; Plenum: New York, NY, USA, 1987; Chapter 1; pp. 9–35.
5. 5. Verhoeven, J.T.J.; Jansen, C.C.C.; Willemen, T.M.; Kox, L.F.F.; Owens, R.A.; Roenhorst, J.W. Natural infections of tomato by Citrus exocortis viroid, Columnea latent viroid, Potato spindle tuber viroid and Tomato chlorotic dwarf viroid. *European J Pl Pathol.* **2004**, 110:823–831.
6. 6. Verhoeven, J.T.J.; Botermans, M.; Meekes, E.T.M.; Roenhorst, J.W. Tomato apical stunt viroid in the Netherlands: most prevalent pospiviroid in ornamentals and first outbreak in tomatoes. *European J Pl Pathol.* **2012**, 133:803–810.
7. 7. Tsushima, T.; Murakami, S.; Ito, H.; He, Y.-H.; Sano, T. Molecular characterization of potato spindle tuber viroid in dahlia. *J Gen Pl Pathol.* **2011**, 77:253–256.
8. 8. Tsuda, S.; Sano, T.; Threats to Japanese agriculture from newly emerged plant viruses and viroids. *J Gen Pl Pathol.* **2014**, 80:2–14.
9. 9. Wang, Y.; Shibuya, M.; Taneda, A.; Kurauchi, T.; Senda, M.; Owens, R.A.; Sano, T. Accumulation of Potato spindle tuber viroid-specific small RNAs is accompanied by specific changes in gene expression in two tomato cultivars. *Virology.* **2011**, 413:72–83.
10. 10. Owens, R.A.; Tech, K.B.; Shao, J.Y.; Sano, T.; Baker, C.J. Global analysis of tomato gene expression during potato spindle tuber viroid infection reveals a complex array of changes affecting hormone signaling. *Mol. Plant Microbe Interact.* **2012**, 25, 582–598.
11. 11. Tsushima, D.; Tsushima, T.; Sano, T. Molecular dissection of a dahlia isolate of potato spindle tuber viroid inciting a mild symptoms in tomato. *Virus Res.* **2016**, 214:11–18.
12. 12. Dou, D.; Zhou, J.M. Phytopathogen effectors subverting host immunity: different foes, similar battleground. *Cell Host & Microbe.* **2012**, 12(4):484–95.
13. 13. Martínez de Alba, A.E.; Elvira-Matelot, E.; Vaucheret, H. Gene silencing in plants: a diversity of pathways. *Biochim Biophys Acta.* **2013**, 1829:1300–1308.
14. 14. Molnar, A.; Melnyk, C.; Baulcombe, D.C.; Silencing signals in plants: a long journey for small RNAs. *Genome Biology.* **2011**, 12:215.
15. 15. Liu, L.; Chen, X. RNA quality control as a key to suppressing RNA silencing of endogenous genes in plants. *Mol. Plant.* **2016**, 9:826–836.
16. 16. Itaya, A.; Folimonov, A.; Matsuda, Y.; Nelson, R.S.; Ding, B. Potato spindle tuber viroid as inducer of RNA silencing in infected tomato. *Mol. Plant-Microbe Interact.* **2001**, 14:1332–1334.
17. 17. Papaefthimiou, I.; Hamilton, A.J.; Denti, M.A.; Baulcombe, D.C.; Tsagris, M.; Tabler, M. Replicating potato spindle tuber viroid RNA is accompanied by short RNA fragments that are characteristic of posttranscriptional gene silencing. *Nucleic Acids Res.* **2001**, 29:2395–2400.
18. 18. Itaya, A.; Zhong, X.; Bundschuh, R.; Qi, Y.; Wang, Y.; Takeda, R.; Harris, A.R.; Molina, C.; Nelson, R.S.; Ding, B. A structured viroid RNA serves as a substrate for dicer-like cleavage to produce biologically active small RNAs but is resistant to RNA-induced silencing complex-mediated degradation. *J Virol.* **2007**, 81:2980–2994.
19. 19. Machida, S.; Yamahata, N.; Watanuki, H.; Owens, R.A.; Sano, T. Successive accumulation of two size classes of viroid- specific small RNAs in potato spindle tuber viroid-infected tomato plants. *Journal of General Virology.* **2007**, 88:3452–3457.
20. 20. Dadami, E.; Boutla, A.; Vrettos, N.; Tzortzakaki, S.; Karakasilioti, I.; Kalantidis, K. DICER-LIKE 4 but not DICER-LIKE 2 may have a positive effect on potato spindle tuber viroid accumulation in Nicotiana benthamiana. *Mol Plant.* **2013**, 6:232–234.

21. 21. Katsarou, K.; Mavrothalassiti, E.; Dermauw, W.; Leeuwen, T.V.; Kalantidis, K. Combined activity of DCL2 and DCL3 is crucial in the defense against potato spindle tuber viroid. *PLoS Pathog.* **2016**, 12: e1005936.
22. 22. Martínez de Alba, A.E.; Flores, R.; Hernández, C. Two chloroplastic viroids induce the accumulation of small RNAs associated with posttranscriptional gene silencing. *J Virol.* **2002**, 76:13094–13096.
23. 23. Di Serio, F.; Gisel, A.; Navarro, B.; Delgado, S.; Martínez de Alba, A.E.; Donvito, G.; Flores, R. Deep sequencing of the small RNAs derived from two symptomatic variants of a chloroplastic viroid: implications for their genesis and for pathogenesis. *PLoS One.* **2009**, 4:7539.
24. 24. Bolduc, F.; Hoareau, C.; St-Pierre, P.; Perreault, J.P. In-depth sequencing of the siRNAs associated with peach latent mosaic viroid infection. *BMC Mol Biol.* **2010**, 11:16.
25. 25. Minoia, S,; Carbonell, A.; Di Serio, F.; Gisel, A.; Carrington, J.C.; Navarro, B.; Flores, R. Specific argonautes selectively bind small RNAs derived from potato spindle tuber viroid and attenuate viroid accumulation in vivo. *J Virol.* **2014**, 88:11933–11945.
26. 26. Gómez, G.; Martínez, G.; Pallás, V. Viroid-induced symptoms in Nicotiana benthamiana plants are dependent on RDR6 activity. *Plant Physiol.* **2008**, 148:414–423.
27. 27. Di Serio, F.; Martínez de Alba, A.E.; Navarro, B.; Gisel, A.; Flores, R. RNA-dependent RNA polymerase 6 delays accumulation and precludes meristem invasion of a viroid that replicates in the nucleus. *J Virol.* **2010**, 84:2477–2489.
28. 28. Adkar-Purushothama, C.R.; Kasai, A.; Sugawara, K.; Yamamoto, H.; Yamazaki, Y.; He, Y.-H.; Takada, N.; Goto, H.; Shindo, S.; Harada, T.; Sano, T. RNAi mediated inhibition of viroid infection in transgenic plants expressing viroid-specific small RNAs derived from various functional domains. *Sci Rep.* **2015**, 5:17949.
29. 29. Carbonell, A.; Martínez de Alba, A.E.; Flores, R.; Gago, S. Double-stranded RNA interferes in a sequence-specific manner with the infection of representative members of the two viroid families. *Virology.* **2008**, 371:44–53.
30. 30. Dalakouras, A.; Dadami, E.; Wassenegger, M. Engineering viroid resistance. *Viruses.* **2015**, 7:634–646.
31. 31. Kasai, A.; Bai, S.; Li, T.; Harada, T. Graft-transmitted siRNA signal from the root induces visual manifestation of endogenous post-transcriptional gene silencing in the scion. *PLoS ONE.* **2011**, 6: e16895.
32. 32. Schwind, N.; Zwiele, M.; Itaya, A.; Ding, B.; Wang, M.; Krczal, G.; Wassenegger, M. RNAi-mediated resistance to Potato spindle tuber viroid in transgenic tomato expressing a viroid hairpin RNA construct. *Plant Pathol.* **2009**, 10:459–469.
33. 33. Wang, M.B.; Bian, X.Y.; Wu, L.M.; Liu, L.X.; Smith, N.A.; Isenegger, D.; Wu, R.M.; Masuta, C.; Vance, V.B.; Watson, J.M.; Rezaian, A.; Dennis, E.S.; Waterhouse, P.M. On the role of RNA silencing in the pathogenicity and evolution of viroids and viral satellites. *Proc. Natl Acad. Sci. USA.* **2004**, 101:3275–3280.
34. 34. Adkar-Purushothama, C.R.; Brosseau, C.; Giguère, T.; Sano, T.; Moffett, P.; Perreault, J.P. Small RNA derived from the virulence modulating region of the potato spindle tuber viroid silences callose synthase genes of tomato plants. *The Plant Cell.* **2015**, 27:2178–2194.
35. 35. Adkar-Purushothama, C.R.; Iyer, P.; Perreault, J.P. Potato spindle tuber viroid infection triggers degradation of chloride channel protein CLC-b-like and ribosomal protein S3a-like mRNAs in tomato plants. *Scientific Reports.* **2017**, 7:8341.
36. 36. Avina-Padilla, K.; Martinez de la Vega, O.; Rivera-Bustamante, R.; Martinez-Soriano, J.P.; Owens, R.A.; Hammond, R.W.; Vielle-Calzada, J.P. In silico prediction and validation of potential gene targets for pospiviroid-derived small RNAs during tomato infection. *Gene.* **2015**, 564:197–205.
37. 37. Eamens, A.L.; Smith, N.A.; Dennis, E.S.; Wassenegger, M.; Wang, M.B. In Nicotiana species, an artificial microRNA corresponding to the virulence modulating region of potato spindle tuber viroid directs RNA silencing of a soluble inorganic pyrophosphatase gene and the development of abnormal phenotypes. *Virology.* **2014**, 450–451, 266–277.
38. 38. Markarian, N.; Li, H.W.; Ding, S.W.; Semancik, J.S. RNA silencing as related to viroid induced symptom expression. *Arch Virol.* **2004**, 149:397–406.
39. 39. Mishra, A.K.; Duraisamy, G.S.; Matoušekm, J.; Radisek, S.; Javornik, B.; Jakse, J. Identification and characterization of microRNAs in *Humulus lupulus* using high-throughput sequencing and their response to *Citrus bark cracking viroid* (CBCVd) infection. *BMC Genom.* **2016,** 17, 919.

40. 40. Navarro, B.; Gisel, A.; Rodio, M.E.; Degado, S.; Flores, R.; Di Serio, F. Small RNAs containing the pathogenic determinant of a chloroplast-replicating viroid guide the degradation of a host mRNA as predicted by RNA silencing. *Plant J.* **2012**, 70, 991–1003.
41. 41. Bernstein, E.; Caudy, A.A.; Hammond, S.M.; Hannon, G.J. Role for a bidentate ribonuclease in the initiation step of RNA interference. *Nature.* **2001**, 409:363.
42. 42. Liu, Q.; Feng, Y.; Zhu, Z. Dicer-like (DCL) proteins in plants. *Functional &Integrative Genomics.* **2009**, 9:277–286.
43. 43. Bartel, D.P. MicroRNAs: Genomics, biogenesis, mechanism, and function. *Cell.* **2004**, 116:281–297.
44. 44. Ramachandran, V.; Chen, X. Small RNA metabolism in Arabidopsis. *Trends Plant Sci.* **2008**, 13:368–374.
45. 45. Xie, M.; Zhang, S.; Yu, B. microRNA biogenesis, degradation and activity in plants. *Cell Mol Lofe Sci.* **2014**, 72(1):87–99
46. 46. Xie, Z.; Johansen, L.K.; Gustafson, A.M.; Kasschau, K.D.; Lellis, A.D.; Zilberman, D.; Jacobsen, S.E.; Carrington, J.C. Genetic and functional diversification of small RNA pathways in plants. *PLoS Biol.* **2004**, 2:642-652.
47. 47. Borsani, O.; Zhu, J.; Verslues, P.E.; Sunkar, R.; Zhu, J.K. Endogenous siRNAs derived from a pair of natural cis-antisense transcripts regulate salt tolerance in Arabidopsis. *Cell.* **2005**, 123:1279–1291.
48. 48. Gasciolli, V.; Mallory, A.C.; Bartel, D.P.; Vaucheret, H. Partially redundant functions of Arabidopsis DICER-like enzymes and a role for DCL4 in producing trans-acting siRNAs. *Curr Biol.* **2005**, 15:1494–1500.
49. 49. Mlotshwa, S.; Pruss, G.J.; Peragine, A.; Endres, M.W.; Li, J.; Chen, X.; Poethig, R.S.; Bowman, L.H.; Vance, V. DICER-LIKE2 plays a primary role in transitive silencing of transgenes in Arabidopsis. *PLoS One.* **2008**, 3:e1755.
50. 50. Bouché, N.; Lauressergues, D.; Gasciolli, V.; Vaucheret, H. An antagonistic function for Arabidopsis DCL2 in development and a new function for DCL4 in generating viral siRNAs. *EMBO J.* **2006**, 25:3347–3356.
51. 51. Vazquez, F.; Blevins, T.; Ailhas, J.; Boller, T.; Meins, F. Evolution of Arabidopsis MIR genes generates novel microRNA classes. *Nucleic Acids Res.* **2008**, 36:6429–6438.
52. 52. Xie, Z.; Allen, E.; Wilken, A.; Carrington, J.C. DICER-LIKE 4 functions in trans-acting small interfering RNA biogenesis and vegetative phase change in Arabidopsis thaliana. *Proc Natl Acad Sci USA.* **2005**, 102:12984–12989.
53. 53. Dunoyer, P.; Voinnet, O. The complex interplay between plant viruses and host RNA-silencing pathways. *Curr Opin Plant Biol.* **2005**, 8:415–423.
54. 54. Rajagopalan, R.; Vaucheret, H.; Trejo, J.; Bartel, D.P. A diverse and evolutionarily fluid set of microRNAs in Arabidopsis thaliana. *Genes Dev.* **2006**, 20:3407–3425.
55. 55. Vazquez, F.; Vaucheret, H.; Rajagopalan, R.; Lepers, C.; Gasciolli, V.; Mallory, A.C.; Hilbert, J.L.; Bartel, D.P.; Crété, P. Endogenous transacting siRNAs regulate the accumulation of Arabidopsis mRNAs. *Mol Cell.* **2004**, 16:69–79.
56. 56. Duc, C.; Sherstnev, A.; Cole, C.; Barton, G.J.; Simpson, G.G. Transcription termination and chimaera RNA formation controlled by Arabidopsis thaliana FPA. *PLoS Genet.* **2013**, 9:e1003867.
57. 57. Liu, F.; Bakht, S.; Dean, C. Cotranscriptional role for Arabidopsis DICER-LIKE 4 in transcription termination. *Science.* **2012**, 335:1621–1623.
58. 58. Deleris, A.; Gallego-Bartolome, J.; Bao, J.; Kasschau, K.D.; Carrington, J.C.; Voinnet, O. Hierarchical action and inhibition of plant Dicer-like proteins in antiviral defense. *Science.* **2006**, 313:68–71.
59. 59. Zhang, C.; Wu, Z.; Wu, J. Biogenesis, function, and applications of virus-derived small RNAs in plants. *Front Microbiol.* **2015**, 6(1273):1–12.
60. 60. Fusaro, A.F.; Matthew, L.; Smith, N.A.; Curtin, S.J.; Dedic-Hagan, J.; Ellacott, G.A. RNA interference inducing hairpin RNAs in plants act through the viral defence pathway. *EMBO Rep.* **2006**, 7:1168–1175.
61. 61. Beauclair, L.; Yu, A.; Bouché, N. microRNA-directed cleavage and translational repression of the copper chaperone for superoxide dismutase mRNA in Arabidopsis. *The Plant J.* **2010**, 62:454–462.
62. 62. Ohta, S.; Mita, S.; Hattori, T.; Nakamura, K. Construction and expression in tobacco of a β-glucuronidase (GUS) reporter gene containing an intron within the coding sequence. *Plant Cell Physiol.* **1990**, 31:805–813.
63. 63. Murray, M.G.; Thompson, W.F. Rapid isolation of high molecular weight plant DNA. *Nucleic Acids Res.* **1980**, 8:4321–4325.

64. 64. Tsushima, D.; Adkar-Purushothama, C.R.; Taneda, A.; Sano, T. Changes in relative expression levels of viroid-specific small RNAs and microRNAs in tomato plants infected with severe and mild symptom-inducing isolates of Potato spindle tuber viroid, *J Gen Pl Pathol.* **2015**, 81:49–62.
65. 65. Suzuki, T.; Fujibayashi, M.; Hataya, T.; Taneda, A.; He, Y.H.; Tsushima, T.; Duraisamy, G.S.; Siglová, K.; Matoušek, J.; Sano, T. Characterization of host-dependent mutations of apple fruit crinkle viroid replicating in newly identified experimental hosts suggests maintenance of stem-loop structures in the left-hand half of the molecule is important for replication. *J Gen Virol.* **2017**, 98:506–516.
66. 66. Bagherian, A.A.A.; Hamzehzarghani, H.; Izadpanah, K.; Djavaheri, M. Effects of potato spindle tuber viroid infection on tomato metabolic profile. *J Pl Physiol.* **2016**, 201:42–53.
67. 67. Zhu, H.; Zhou, Y.; Castillo-González, C.; Lu, A.; Ge, C.; Zhao, Y.T.; Duan, L.; Li, Z.; Axtell, M.J.; Wang, X.J.; Zhang, X. Bidirectional processing of pri-miRNAs with branched terminal loops by Arabidopsis Dicer-like1. *Nat Struct Mol Biol.* **2013**, 20(9):1106-15
68. 68. Hill, J.M.; Lukiw, W.J. Comparing miRNAs and viroids; highly conserved molecular mechanisms for the transmission of genetic information. *Frontiers in Cellular Neuroscience.* **2014**, 8(45).
69. 69. Hill, J.M.; Zhao, Y.; Bhattacharjee, S.; Lukiw, W.J. miRNAs and viroids utilize common strategies in genetic signal transfer. *Frontiers in Molecular Neuroscience.* **2014**, 7(10).
70. 70. Campos, L.; Granell, P.; Tárraga, S.; López-Gresa, P.; Conejero, V.; Bellés, J.M.; Rodrigo, I.; Lisón, P. Salicylic acid and gentisic acid induce RNA silencing-related genes and plant resistance to RNA pathogens. *Plant Physiol Biochem.* **2014**, 77:35–43.
71. 71. Juszczak, I.; Baier, M. The strength of the miR398-Csd2-CCS1 regulon is subject to natural variation in Arabidopsis thaliana. *FEBS Letters.* **2012**, 586:3385–3390.
72. 72. Ren, L.; Guiliang, T.G. Identification of sucrose-responsive microRNAs reveals sucrose-regulated copper accumulations in an SPL7-dependent and independent manner in Arabidopsis thaliana. *Plant Science.* **2012**, 187:59–68.
73. 73. Schnölzer, M.; Haas, B.; Ramm, K.; Hofmann, H.; Sänger, H.L. Correlation between structure and pathogenicity of potato spindle tuber viroid (PSTV). *EMBO J.* **1985**, 4:2181–2190.
74. 74. Sano, T.; Candresse, T.; Hammond, R.W.; Diener, T.O.; Owens, R.A. Identification of multiple structural domains regulating viroid pathogenicity. *Proc. Natl. Acad. Sci. USA.* **1992**, 89:10104–10108.
75. 75. Zheng, Y.; Wang, Y.; Ding, B.; Fei, Z. Comprehensive transcriptome analyses reveal that potato spindle tuber viroid triggers genome-wide changes in alternative splicing, inducible trans-acting activity of phased secondary small interfering RNAs, and immune responses. *J Virol.* **2017**, 91:e00247–17.
76. 76. Xia, C.; Li, S.; Hou, W.; Fan, Z.; Xiao, H.; Lu, M.; Sano, T.; Zhang, Z. Global transcriptomic changes induced by infection of cucumber (*Cucumis sativus L.*) with mild and severe variants of hop stunt viroid. *Front. Microbiol.* **2017**, 8:2427.
77. 77. Spitzer, M.; Wildenhain, J.; Rappsilber, J.; Tyers, M. BoxPlotR: a web tool for generation of box plots. *Nat Methods.* **2014**, 11:121–122.